Key Engineering Materials
ISSN: 1662-9795, Vol. 1047, pp 347-358

Submitted: 2026-01-20
Accepted: 2026-02-11
Online: 2026-04-13

Effects of Current Density during Electrically Assisted Friction Stir Additive Manufacturing Hole Repair of AA 7075 on a Conventional Machine

Laura L. Catalano[1,2,a*], Cordelia M. Norris[2,b], Elizabeth M. Mamros[3,c] and John T. Roth[1,2,d]

[1]Department of Mechanical Engineering, University of New Hampshire, Durham, NH 03824, USA

[2]John Olson Advanced Manufacturing Center, University of New Hampshire, Durham, NH 03824, USA

[3]Department of Mechanical Engineering, Bucknell University, Lewisburg, PA 17837, USA

[a*]laura.catalano@unh.edu, [b]cordelia.norris@unh.edu, [c]elizabeth.mamros@bucknell.edu, [d]john.roth@unh.edu

Keywords: aluminum, friction stir additive manufacturing (FSAM), electrically assisted, hole repair.

Abstract. Of interest for military applications is the repair of damaged fastener holes on aircraft. One of the preferred repair processes, specifically for aluminum alloy 7075 (AA 7075), is friction stir additive manufacturing (FSAM) to avoid hot cracking and high residual stresses. Some of the largest challenges with this additive manufacturing process, however, are the high axial force requirement to deposit the consumable tool onto the substrate material as well as the amount of downtime necessary for repair. One possible solution is the utilization of electrical assistance during the FSAM process, since the yield strength of the alloy decreases with increasing current density when depositing bar stock. This work investigates utilizing electrically assisted friction stir technology on a conventional knee mill, which is commonly used in depots and machine shops, to showcase that repairs can be completed on commercial, commonly available equipment with decreased repair time. Varying current addresses an efficiency challenge of additive manufacturing by lowering the dwell time necessary for deposition. While higher current densities would address one of the largest concerns of FSAM – the high force requirements, the ability to repair holes using a retrofit conventional system would allow for more point-of-need applications. With the eventual application of military interest in mind, 7.95 mm (5/16”) diameter holes are drilled and repaired using FSAM via a conventional Bridgeport knee mill for use in typical machine shop locations. The material properties of AA 7075 stock material are compared to FSAM hole repairs completed with and without electricity incorporated.

Introduction

Additive manufacturing (AM) is comprised of seven processes, as listed by the American Society for Testing and Materials (ASTM), which include binder jetting, directed energy deposit (DED), material extrusion, material jetting, powder bed fusion (PBF), sheet lamination, and vat photopolymerization [1]. Fusion-based AM (i.e., DED and PBF) is notably one of two methods for metal additive manufacturing (MAM). In this process, the material reaches melting temperature during deposition onto a substrate, resulting in high heating and cooling rates, which affect the microstructure and lead to high residual stresses based on thermal gradients [2]. To decrease the amount of residual stresses and deposit material at temperatures below the metal’s melting point, another method of MAM was introduced: solid state additive manufacturing (SSAM).

One class of SSAM includes friction stir additive manufacturing (FSAM), developed on the basis of friction stir welding. The first written account of friction joining was a patent by White, filed in 2000 [3]. This process was further developed by Allison and Jordon in 2017, enabling grain refinement, lower residual stresses, and material properties comparable to those of untreated material [4]. The process utilizes a rotating tool, containing a feedstock that is deposited onto a traversing substrate, where friction is produced to generate heat for deposition. Peak temperatures during this

process reach approximately 60% to 90% of the melting temperature for the material, allowing better deposition properties than fusion-based AM due to the elimination of the solidification step [5]. Specifically, using AA 7075, FSAM proved to be sufficient for repairs due to fewer kissing bonds and no sharp interface between the deposition and the wall of the hole compared to fusion-based AM.

Repairs were completed using FSAM with AA 7075 by Virginia Tech in 2019, including single-through hole fillings, double-through hole fillings, and grooves [6]. Post-repair testing found that the material properties (e.g., hardness and microstructure) were comparable to the as-received material's properties. FSAM repairs using AA 7075 have also been explored for holes produced by ammunition rounds in 2022 [7]. This work investigated the repair of a damaged ballistic hole and the reproduction of the hole to compare the properties of the damage location and surface to control plates just penetrated by full metal jacket (FMJ) rounds. Ultimately, the authors observed noticeable surface damage among these new holes, but the material properties remained similar to the controls. One noticeable limiting attribute of using FSAM, especially in the case of AA 7075, is the need for larger forging forces to reduce defects, allowing for less variability in the microstructure [8].

Studies previously completed by Roth et al. promote the use of electrical assistance to reduce the necessary loading [9]. The use of electrical assistance allows for the yield strength and deformation resistance of the material to decrease, achieving best performance when current density reaches between 50 A/mm^2 and 90 A/mm^2 for AA 7075-T6. This study utilized small cylindrical specimens (9.5 mm height with a 6.4 mm diameter) for comparisons of compressive forces with varying degrees of electrical assistance. Another notable study was performed by the Yancheng Institute of Technology, focusing on the mechanical properties of AA 7075-T6 while completing electrically assisted forming [10]. Friction stir welding has also utilized the Joule heating method to improve the material's viscoplasticity and eliminate defects [11]. However, the incorporation of electrical assistance has not yet been studied for FSAM.

Electrically assisted FSAM would aid more conventional repairs, as decreasing the dwell time would allow for more efficiency, lowering the necessary downtime. This eventually could have military applications for in-situ, on-vehicle repairs with even shorter downtimes from higher levels of electrical assistance. A repair methodology has been investigated by Baylor University, using AA 7050 to determine the effects of the tool offset on the material flow and final deposition for aircraft repair [12]. This study focused on filling pre-machined grooves and comparing the resulting material properties to the as-received material. Notably, 7xxx series aluminum was employed for its high strength and is typically used for primary structures in aircraft, despite being difficult to repair due to material changes during deposition and high force requirements [13]. Current work focuses on the use of electrical assistance to lower dwell time on commercial, off-the-shelf machines, such as a conventional knee mill, for higher efficiency of repair. The addition of low levels of current density indicates that the assistance impacts the dwell time. This also considers the machinery in most manufacturing shops, as common welding equipment would have low amperage.

This paper describes the use of electrical assistance with varying current densities to decrease the time required for repairs of a 7.95 mm (5/16") diameter hole in AA 7075, completed on a knee mill. Repairs were subject to current densities ranging from 0 A/mm^2 to 11.84 A/mm^2 (range of 0 – 1500 A), to determine the effects of current on larger specimens. The maximum process temperature and axial force were recorded. The material hardness of the repairs was compared to the as-received material.

Materials and Methods

The as-received material properties of both the plates and the consumable stock are shown in Table 1, as provided by the supplier. Both the substrate plates and consumable stock tooling were AA 7075-T6, utilized for repair on a knee mill.

Table 1. Chemical Composition, Ultimate Tensile Strength (UTS), and Yield Tensile Strength (YTS) of AA 7075-T6 for Substrate and Consumable Tooling, Supplied by Kaiser Aluminum.

	Chemical Composition (%)											UTS (MPa)	YTS (MPa)
Material	Al	Cr	Cu	Fe	Mg	Mn	Si	Ti	Zn	Zr	V		
As-Received 7075-T6 Plates	89.36	0.2	1.5	0.22	2.6	0.03	0.09	0.03	5.9	0.02	0	584.7	516.4
As-Received 7075-T6 Rod	89.68	0.2	1.5	0.15	2.5	0.03	0.06	0.03	5.8	0.01	0.01	568.1	514.3

Friction Stir Additive Manufacturing (FSAM).

Experiments were completed using a 1994 EZ-Trak Bridgeport knee mill to show the accessibility of implementing FSAM technologies. The substrate, 3.175 mm (1/8”) thick plates of AA 7075, were clamped to the mill’s table while the consumable tooling, consisting of 12.7 mm (1/2”) diameter and 101.6 mm (4”) in length rod stock, was held within a collet in the head of the Bridgeport and fastened using the quill and drawbar. Several 7.95 mm (5/16”) diameter holes were produced in the substrate using a waterjet for repair. In this repair process, the rotating feedstock was plunged at the side of the hole, approximately 19.05 mm (3/4”) away. Dwelling then occurred until the rotating stock reached a temperature of ~70% of the material’s melting point (~445°C) before the table of the mill was manually traversed, allowing for the deposition to fill the hole, as shown in Figure 1. Manual traversing was completed to prove that automation is not necessary for FSAM. Note that this experimentation was completed using the same operators for consistent results. Other constant parameters for experiments are shown in Table 2.

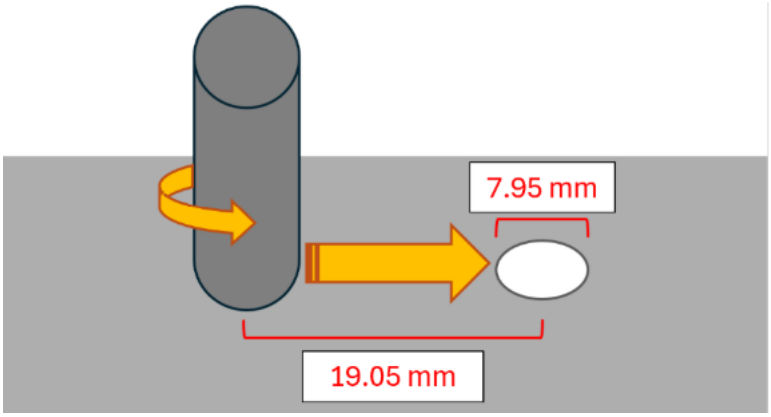

Fig. 1. Schematic of Experimentation Procedure for FSAM.

Table 2. Constant Parameters for Experimentation.

Parameter	Constant Value
Spindle Speed	2000 rpm
Bridgeport Head Tilt	0°
Hole Diameter	7.95 mm
Plate Thickness	3.175 mm
Consumable Tool Diameter	12.7 mm
Consumable Tool Initial Length	101.6 mm
Tool Initial Distance From Hole	19.05 mm

Maximum temperature during deposition was recorded using a FLIR A700 infrared camera mounted to a tripod within a meter of the experiment. Emissivity was set for the camera to be 0.3 due to the aluminum material being a rough surface from deposition and expected temperatures to be approximately 400°C [14]. The dwell time was determined from video footage captured by a separate camera placed next to the IR camera, with a frame rate of 60 fps and a resolution of 1080 pixels. Force data was also collected during experiments using two 50 kN ATO load cells shown in Figure 2.

Electrical Assistance.

The two load cells were clamped to the mill table and placed under the experimental setup to collect output force data in the z-direction. Between the load cells and the 7075 substrate, a 12.7 mm (½") thick ceramic plate was placed to provide electrical isolation of the load cells from the workpiece.

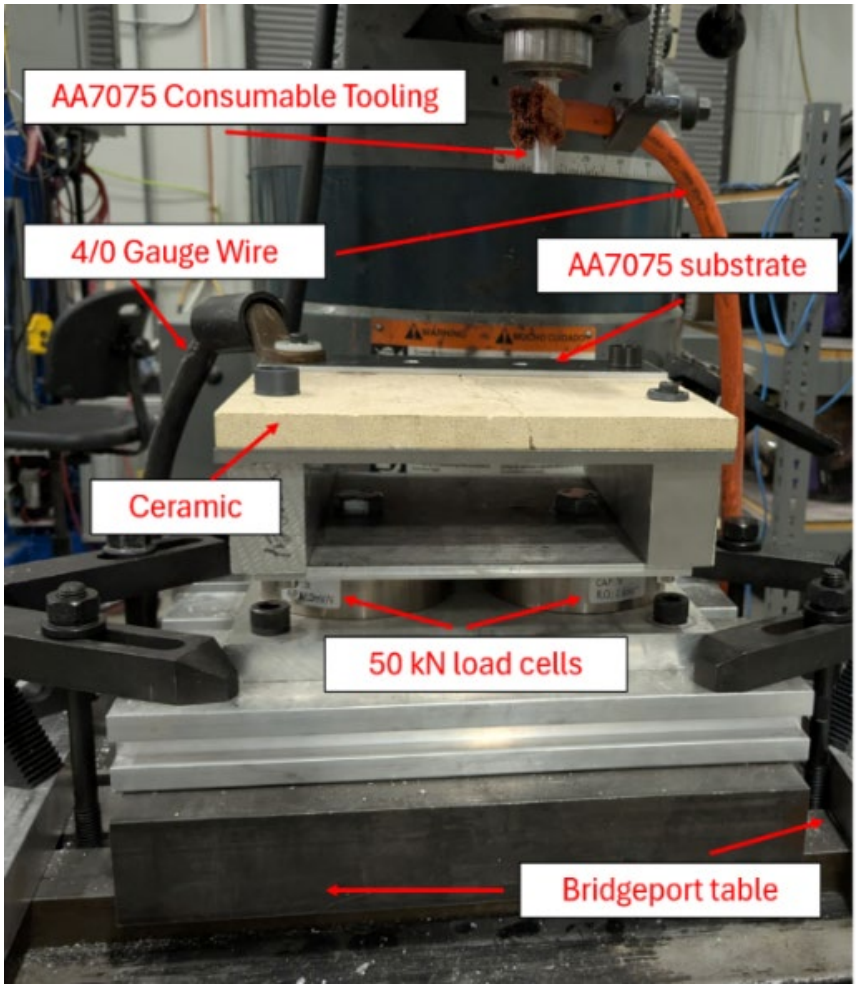

Fig. 2. Experimental Setup for FSAM Using Electrical Assistance on Conventional Bridgeport Knee Mill.

Another critical component for electrical isolation, to separate the consumable tooling from the Bridgeport head, was the use of a hollow, ceramic cylinder (50 mm length) with a G10 (fiberglass-epoxy composite) backing placed within an R8 collet inside of the spindle as shown in Figure 3.

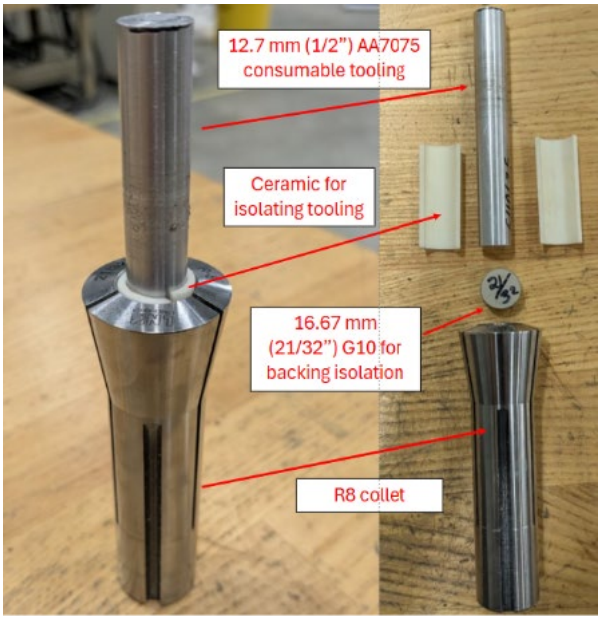

Fig. 3. Electrical Isolation of the Collet for the AA 7075 Consumable Tooling, Using Ceramic and G10.

To add electrical assistance, a 6000 A power supply (ATO), with two 4/0-gauge welding wires, was incorporated to deliver power to the setup, which can be seen in Figure 4. One wire was attached to the substrate while the other wire surrounded the rotating bar stock for deposition, positioned so as to not produce a magnetic field that would impact the deposit. Note that the wire attached to the substrate was also electrically isolated using a polylactic acid (PLA) washer.

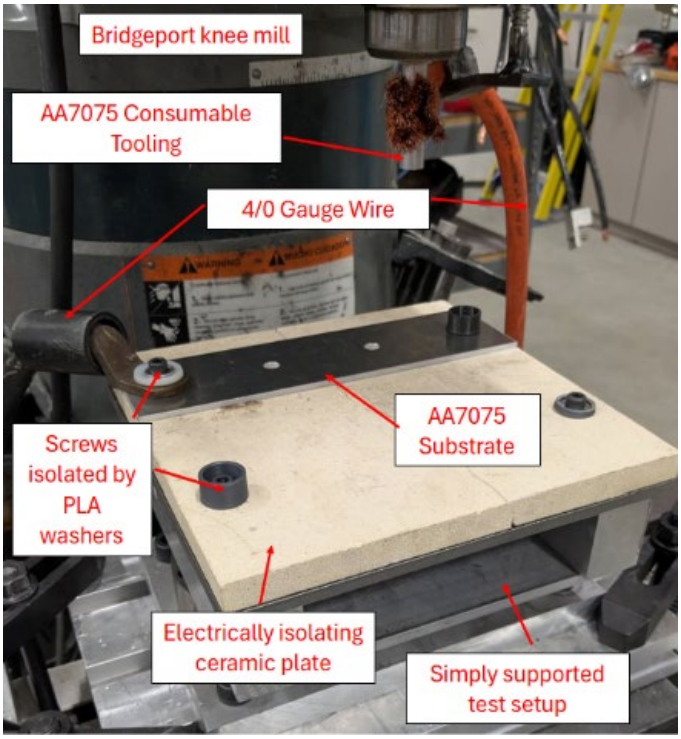

Fig. 4. Setup of Substrate Attached to Simply Supported Test Setup for Electrical Isolation.

The varying currents and corresponding densities utilized for experimentation are shown in Table 3. These current values were defined using the control panel of the ATO power supply and were confirmed using both an ammeter and the output current shown on the control panel's display. Current densities, from these values were calculated using Equation 1. Experimentation was conducted up to three times for each density to confirm repeatability, and two specimens extracted from the region of the substrate with no holes or repairs were used for controls for comparison.

Table 3. Experimentation Currents and Corresponding Current Densities.

Current (A)	Current Density (A/mm^2)
0	0
500	3.95
1000	7.89
1500	11.84

$$\text{Density} = \frac{\text{Current}}{\text{Cross-Sectional Area of Tool}} \quad (1)$$

Sample Preparation and Analysis.

Each experiment was labeled and prepped for hardness testing for comparison of material properties. The sides of deposition of the samples were machined flat using a 9.525 mm (3/8") diameter end mill and then the plates were cut into squares with side lengths less than 20 mm using a vertical bandsaw, noting the transverse direction upon completion. Specimens were labeled with applied current and directions before being mounted in 1.25-inch Allied EpoxySet pucks. Once set and removed from casings, the repair samples were placed in a Buehler Ecomet 3 for grinding and polishing using silicon carbide abrasive disks ranging from 180 to 1200 grit. Specimens were then placed on diamond polishing disks with suspension particle sizes of 9 μm and 2 μm to achieve mirror finishes.

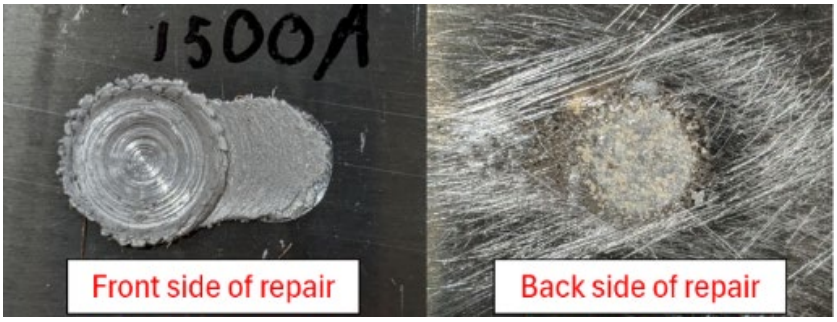

Fig. 5. Representative of the Front (Deposition) and Back (Opposite) Side of a Repair Prior to Milling Flat (Example Shown is from a 1500 A Experiment).

After polishing, samples were placed under a KLA iMicro Nanoindenter for hardness data collection. An array of seven points was selected to include the outside of the hole, the edges, and the center of each sample, as shown in Figure 6. Points were evenly spaced 2 mm apart at the horizontal centerline of the hole repair. Two additional samples of the substrate material without repair were also measured to establish a control hardness value. Specimens from each current density were put under the iMicro in a random order, all utilizing the same pattern of points.

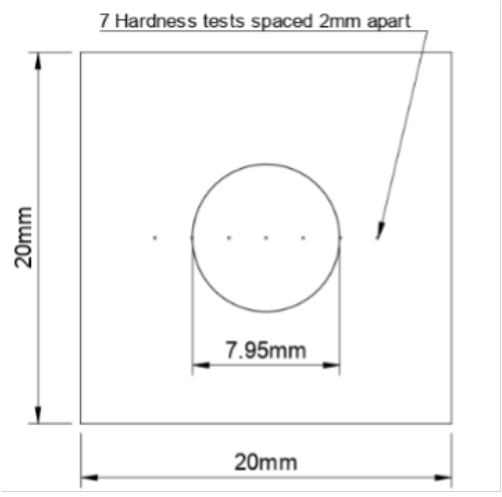

Fig. 6. Diagram of Locations for Hardness Testing Points of Filled Repair of AA 7075 Using KLA Instruments iMicro Nanoindenter.

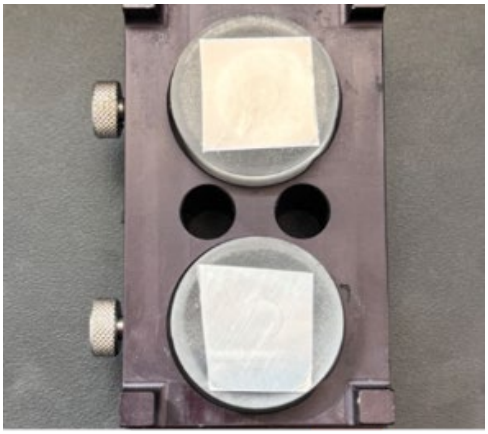

Fig. 7. Representative Samples of Hardness Testing of Filled Repair of AA 7075 Using the KLA Instruments iMicro Nanoindenter (Pucks Shown are from 1500 A Experiments).

Results and Discussion

Results from the experiments are organized in order of amperage for viewing purposes, however, note that experimentation was completed in a random order to minimize bias. Outputs collected during experiments include the dwell time, maximum loading while traversing, and maximum temperature. The effect of varying currents on these outputs was explored using JMP statistical software [14].

Effects of Current Density on Dwell Time.

Using JMP, regression analyses were conducted, and the varying currents were plotted against their corresponding dwell times. Dwell time was established as the time from when the rotating bar stock touched the plate until there was the beginning of a layer of buildup on the substrate before traversing, typically noted by an audible change in sound during the experiment. This change was determined by videos captured using a camera, noted previously to have a rate of 60 fps. This dwell time also corresponded to the time required to allow enough heat to be generated by the friction between the rotating bar stock and the substrate to deposit the rod onto the plate. As shown in Figure 7, the dwell time decreases with increasing current, as at 0 amperes the dwell lasts for 60-99 seconds while at a higher current (i.e., 1500 amperes), the dwell time only lasts up to 30 seconds. Significance was noted for this impact of current on dwell time in the software, as the p-value from the testing completed (0.0092) was much less than 0.05.

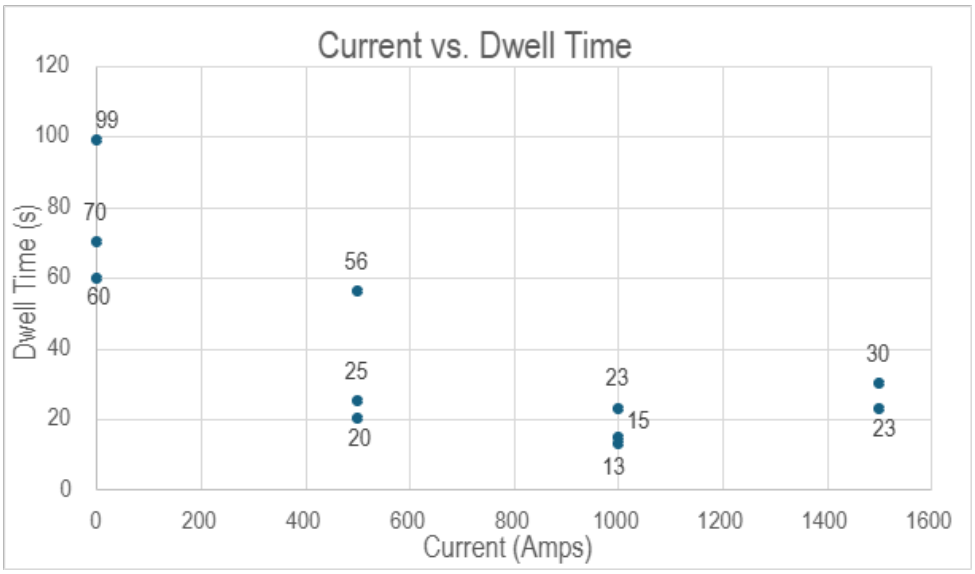

Fig. 8. Regression Plot Showing the Effect of Current (Amperes) on Dwell Time (s).

The use of low current densities, to prove the ability to complete testing on typical machine shop equipment, shows a steady decrease in dwell time. With higher currents, this dwell time would likely decrease further allowing for almost immediate deposition.

Effects of Current on Maximum Loading.

From JMP's regression plot for the impact of current on maximum loading during traverse, there appears to be a slight downward trend in Figure 8. Values for experiments performed at 1500 amperes skew the data upwards slightly, but traverse rate was controlled manually, enabling error in force results. Such traversing was completed using the same operators throughout testing to produce as minimal irregularity as possible. The traverse rate was also noted to reach its peak when traversing out of the filled hole. Meanwhile, the effect of current on maximum loading shows little indication of significance as the p-value calculated was 0.1358, which is higher than expected. Excluding the experiments completed with 1500 amperes, the p-value for the rest of the data proves the effect of current on maximum loading to be significant, with a value of 0.0223.

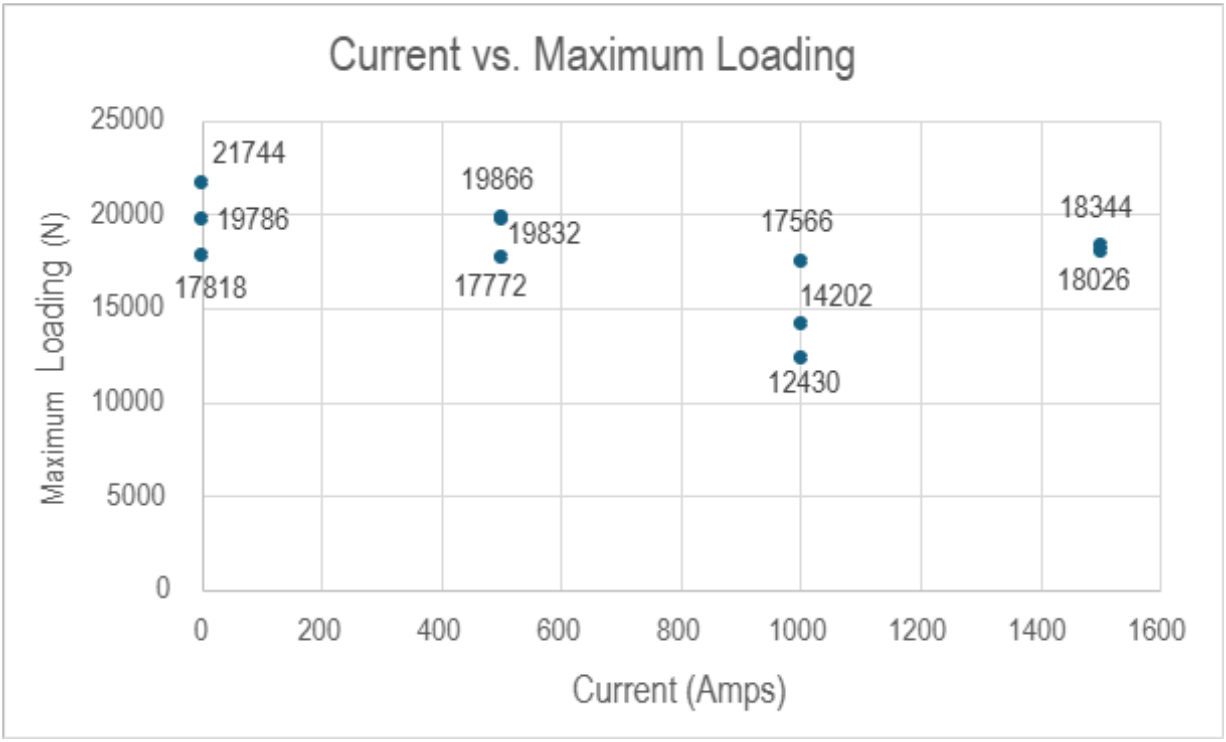

Fig. 9. Regression Plot Showing the Effect of Current (Amperes) on Maximum Loading (N).

Effects of Current on Maximum Temperature.

The manual method of traverse was expected to cause some variation in the resulting temperatures, based on FSAM occurring at temperatures between 60-90% of the melting point for AA 7075. This was confirmed through the maximum temperatures during experimentation for each sample being between 420 °C and 530 °C, with approximately 100°C of variation for the 0 A experiments. The high p-value of 0.8881 indicating no significant effects also validated this idea. It was noted that the variation in the temperature was a result of the differences in dwell time, where an increase of dwell time typically corresponds to an increase in load and temperature.

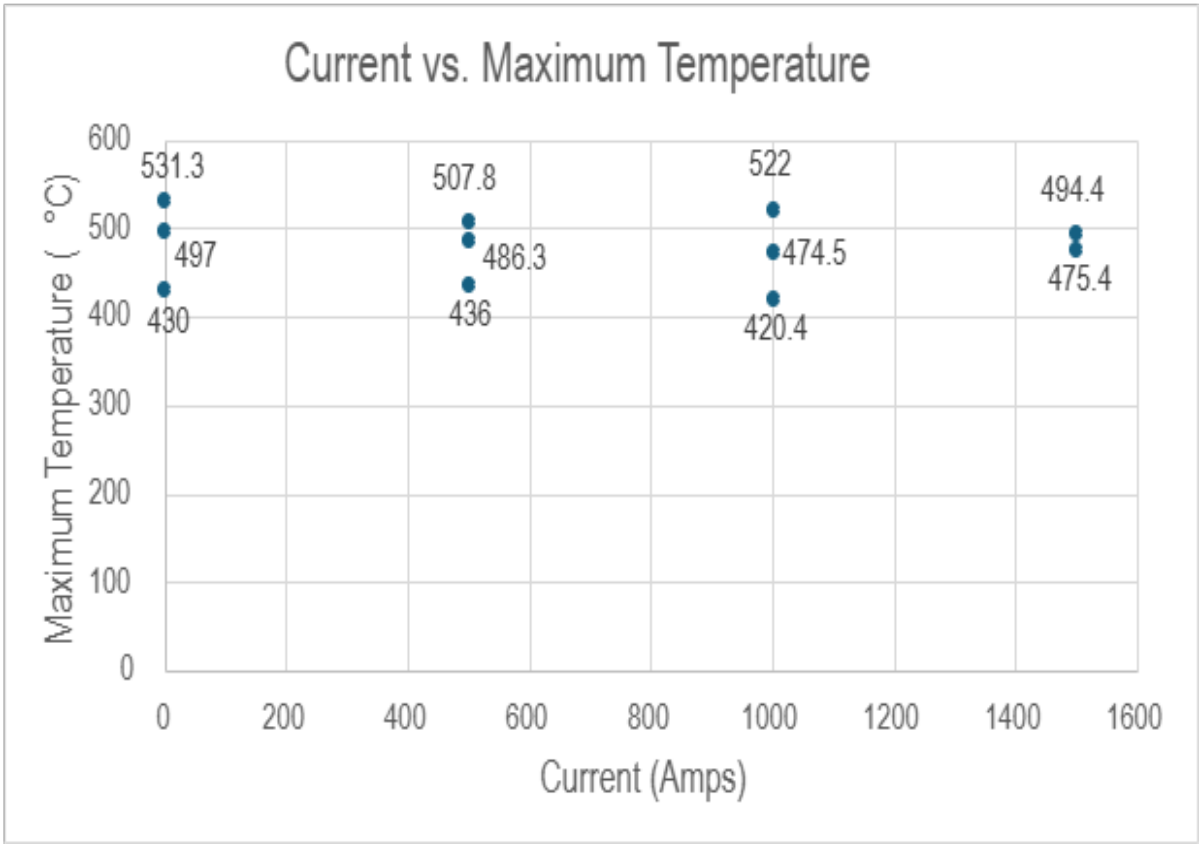

Fig. 10. Regression Plot Showing the Effect of Current (Amperes) on Maximum Temperature (°C).

Desirability functions reveal the trend of higher currents minimizing the loading, as supported by the author's previous work [9]. The decreasing load is also impacted by a shorter dwell time. The Prediction Profiler in JMP provides optimal settings for the minimization of maximum load based on previous data, utilizing the geometric mean from each individual response. The minimize desirability function incorporates a three-part piecewise function that interpolates cubic functions regarding the low, middle, and high values as well as the exponential in the tails. From JMP, the optimal settings consist of a current of 1500 amperes and a dwell time of 13 seconds to produce a load of approximately 16 kN. The basis of this conclusion stems from the decrease of load within the range of 0 to 1000 amperes. This optimization has a desirability of 0.55 based on the eight data points from experimentation. This value would likely increase with more experiments conducted over a larger current range.

Effects of Current on Material Hardness.

Hardness results showed a correlation between applied current and average hardness across all seven points over the region of repair. As seen in Figure 10, the average Vickers hardness increased from 157.95 at 0 amperes to a peak of 178.71 at 1000 amperes. A slight decrease was observed at 1500 amperes, with an average hardness of 175.10. This suggests that increased current density correlates with higher hardness values. The p-value (0.3439) from JMP indicates no significance of the effects of current on Vickers hardness, as the value is higher than 0.05. Further testing at higher current densities would assist in confirming significance. The average hardness of the as-received material was approximately 211.7 HV while the peak average hardness (at 1000 amperes) of 178.71 HV is 15.6% lower than the control hardness.

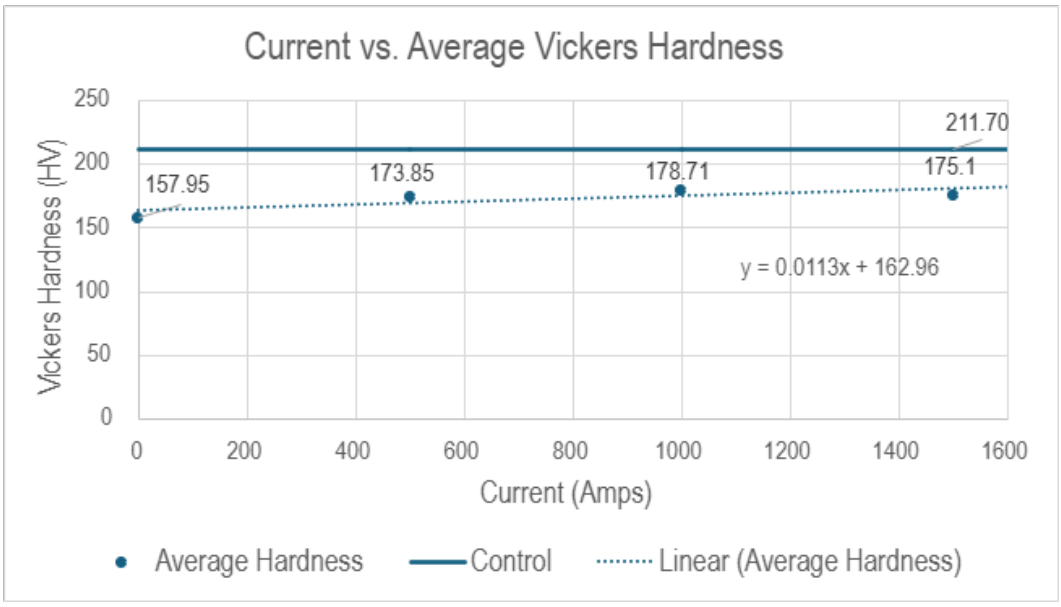

Fig. 11. Regression Plot Showing the Effect of Current (Amperes) on Average Hardness (HV).

The hardness data was collected at the seven locations shown in Figure 6, which is presented in Figure 12. Although a clear overall trend was not discernable, the hardness values remained between 141 and 207 HV.

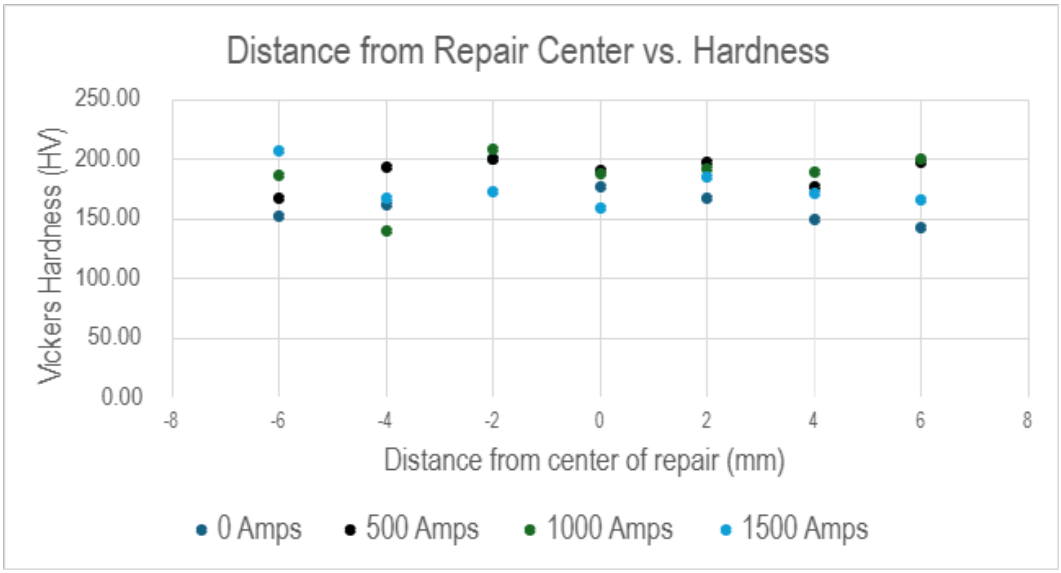

Fig. 12. Plot of the Effect of Distance from the Repair Center (mm) on Hardness (HV) with Shading to Indicate the Hole Location.

The repair center hardness (point 4 in Figure 12) showcases a contrasting trend between the current and the center hardness. Hardness at the center decreased consistently with increasing current: from 176 at 0 amperes to 158.25 at 1500 amperes. This inverse trend, shown in Figure 11, suggests that heating near the tool center may reduce hardness. Meanwhile, hardness at points adjacent to the center, at ±2mm and ±4mm, showed higher values with increased current. For example, at ±2mm, the hardness rose from an average at the center of 168 HV to approximately 180 HV. There was no noticeable significance of the effect of the current on the hardness of the repair center, as the p-value determined was 0.4597.

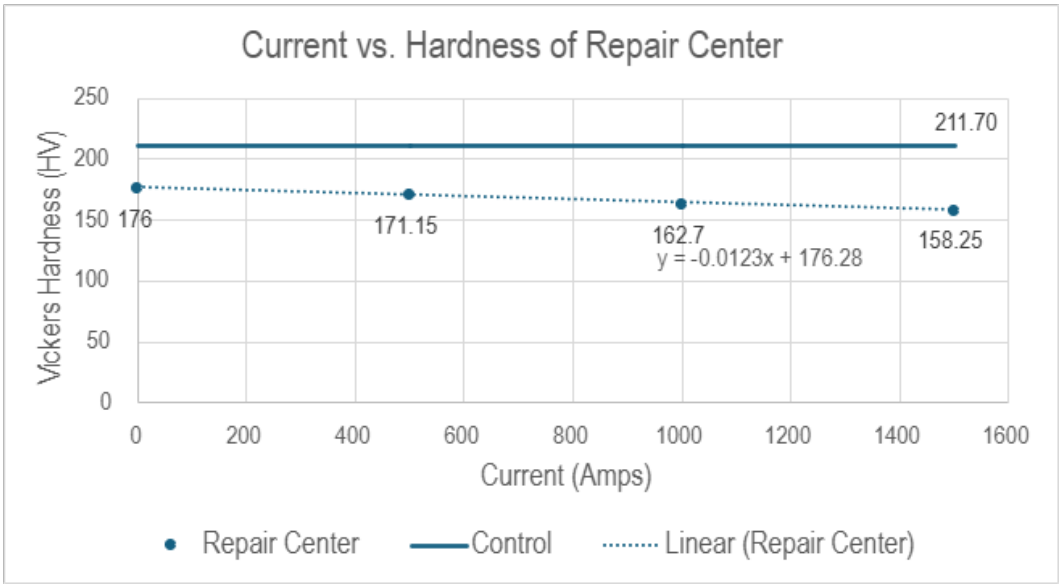

Fig. 13. Regression Plot Showing the Effect of Current (Amperes) on Average Hardness (HV) at the Repair Center.

Conclusion

In this work, FSAM repairs were completed for AA 7075 using a traditional knee mill with electrical assistance for currents ranging from 0 A to 1500 A. The effects of current on the maximum force, maximum temperature, dwell time, and hardness near the repair location were investigated. The effect of dwell time on current was found to be statistically significant, with the dwell time decreasing as current increased. The maximum load was also found to decrease with increasing current. The maximum temperature did not appear to be impacted by the electrical assistance, as expected. The average hardness increased with increasing current, but the hardness measured at the center of the repair decreased slightly. In conclusion, the use of electrical assistance during FSAM is an effective strategy to reduce the dwell time necessary for repair, without a significant effect on the hardness of the material. This work also showcases the ability to complete repairs using standard machine shop equipment, including traditional welders and knee mills, and achieve similar properties to the original substrate.

Future work will include conducting experiments at larger amperage conditions to observe under what conditions the trends shown in this work start to deviate. The effects of electrical assistance on FSAM process parameters, e.g., spindle speed and plunge rate, will also be investigated.

Acknowledgement

The authors would like to thank Owen Mahanes, Alannah Ross, Maya More, and Haydn Jankowski (UNH) for their assistance in conducting experiments, Dr. Benjamin Mitchell (UNH) for assistance with the electrical setup, and Shawn Banker (UNH) for assisting with the hardness measurements. Additionally, the authors wish to thank Professors J. Brian Jordon and Paul Allison of university partner, Baylor University, and Pin Lu and Aaron Birt of industry partner, Solvus Global, for their advice on the experiments. The authors would also like to gratefully acknowledge the financial support of the U.S. Army Research Lab (ARL) and the National Center for Manufacturing Sciences (NCMS), project number 2023166-142357. The KLA iMicro Nanoindenter used is managed by the University Instrumentation Center (UIC) and was purchased with funds from the US National Science Foundation (NSF) EPSCoR RII program (Grant OIA-1757371) awarded to the New Hampshire Center for Multiscale Modeling and Manufacturing of Biomaterials (NH BioMade).

References

[1] Additive manufacturing-General principles-Fundamentals and vocabulary. (n.d.). https://store.astm.org/f3177-21.html.

[2] Collins, P.C., D.A. Brice, P. Samimi, I. Ghamarian, and H.L. Fraser. “Microstructural Control of Additively Manufactured Metallic Materials.” Annual Review of Materials Research. Annual Reviews, 2016. https://doi.org/10.1146/annurev-matsci-070115-031816.

[3] White, Dawn. Object Consolidation Employing Friction Joining, issued October 1, 2002.

[4] Rivera, O. G., P. G. Allison, J. B. Jordon, O. L. Rodriguez, L. N. Brewer, Z. McClelland, W. R. Whittington, et al. “Microstructures and Mechanical Behavior of Inconel 625 Fabricated by Solid-State Additive Manufacturing.” Materials Science and Engineering: A 694 (2017): 1–9. https://doi.org/10.1016/j.msea.2017.03.105.

[5] Mishra, R. S., and Z. Y. Ma. “Friction Stir Welding and Processing.” Materials Science and Engineering: R: Reports 50, no. 1 (2005): 1–78. https://doi.org/10.1016/j.mser.2005.07.001.

[6] Griffiths, R. Joey, Dylan T. Petersen, David Garcia, and Hang Z. Yu. “Additive Friction Stir-Enabled Solid-State Additive Manufacturing for the Repair of 7075 Aluminum Alloy.” Applied Sciences 9, no. 17 (2019). https://doi.org/10.3390/app9173486.

[7] Stubblefield, George, M. Williams, J. Tew, R. Rowe, M. Barkey, J. Jordon, and Paul Allison. “Ballistic Evaluation of Aluminum Alloy (AA) 7075 Plate Repaired by Additive Friction Stir Deposition Using AA7075 Feedstock.” Journal of Dynamic Behavior of Materials 9 (December 2022). https://doi.org/10.1007/s40870-022-00363-6.

[8] He, Changshu, Ying Li, Zhiqiang Zhang, Jingxun Wei, and Xiang Zhao. “Investigation on Microstructural Evolution and Property Variation along Building Direction in Friction Stir Additive Manufactured Al–Zn–Mg Alloy.” Materials Science and Engineering: A 777 (February 2020): 139035. https://doi.org/10.1016/j.msea.2020.139035.

[9] Perkins, Timothy A., Thomas J. Kronenberger, and John T. Roth. “Metallic Forging Using Electrical Flow as an Alternative to Warm/Hot Working.” Journal of Manufacturing Science and Engineering 129, no. 1 (June 14, 2006): 84–94. https://doi.org/10.1115/1.2386164.

[10] Dou, Shasha, Zhuang Liu, Zhijun Li, Haojie Shi, Kang Zhou, and Jiansheng Xia. 2025. "Mechanical Properties of 7075-T6 Aluminum Alloy in Electrically Assisted Forming" Metals 15, no. 2: 117. https://doi.org/10.3390/met15020117.

[11] Santos, Telmo G., R.M. Miranda, and Pedro Vilaça. “Friction Stir Welding Assisted by Electrical Joule Effect.” Journal of Materials Processing Technology 214, no. 10 (October 1, 2014): 2127–33. https://doi.org/10.1016/j.jmatprotec.2014.03.012.

[12] Rojas, Victor A., Ismael Y. Hidalgo, Khaled Matalgah, Trevor J. Fleck, Luke N. Brewer, Gregory W. Kubacki, J. Brian Jordon, and Paul G. Allison. 2025. "Elucidating the Effects of Material Flow from Deposition Offset on AFSD Repair of AA7050" Metals 15, no. 2: 164. https://doi.org/10.3390/met15020164.

[13] Su, J.-Q, T.W Nelson, R Mishra, and M Mahoney. “Microstructural Investigation of Friction Stir Welded 7050-T651 Aluminium.” Acta Materialia 51, no. 3 (February 7, 2003): 713–29. https://doi.org/10.1016/S1359-6454(02)00449-4.

[14] “Emissivity - Metals | Fluke Process Instruments.” https://www.flukeprocessinstruments.com/en-us/service-and-support/knowledge-center/infrared-technology/emissivity-metals.

[15] 2025 JMP® Version 18.0.2. JMP Statistical Discovery LLC, Cary, NC.